# Achieving Uniform In-Plane B1 Amplitude in a 3D Volume for High Field MRI: A Computer Simulation Study

Z. J. Wang[1,2], Z. Chu[1,2]

[1]Texas Children's Hospital, Houston, Texas, United States, [2]Baylor College of Medicine, Houston, Texas, United States

## Introduction

Achieving uniform RF excitation in high field MRI scanners is desirable. Although a totally homogeneous $B_1$ field is unattainable [1], allowing phase variation in space can lead to improvement in the $B_1$ amplitude [2,3]. For a lossy uniform medium, in-plane homogeneous $B_1$ amplitude distribution in a 3D volume is allowed by Maxwell's equations. However, the field distribution is strongly affected by the shape of the object, and conventional hardware configurations are unable to provide optimal results. Using multiple-port variable-driven TEM resonator, highly uniform $B_1$ amplitude has been demonstrated for ultra high field MRI in a transverse slab [4]. Here, we investigate the use of an array transmit coil using computer simulations. An analytic target $B_1$ field pattern with uniform in-plane amplitude was generated in a human head model from the RF fields of individual current loops.

## Methods

We attempt to generate circularly polarized (CP) RF field inside the sample given as:

$$B_{1x} = B_1 \cdot \cos(k_2 x) \cdot e^{ik_1 y} \qquad B_{1y} = i \cdot B_1 \cdot \cos(k_2 x) \cdot e^{ik_1 y} \qquad B_{1z} = B_1 \cdot (z - z_0) \cdot [k_2 \cdot \sin(k_2 x) + k_1 \cdot \cos(k_2 x)] \cdot e^{ik_1 y} \quad (1)$$

Here, $k_1$ is real, $k_1$ and $k_2$ satisfy $k_1^2 + k_2^2 = k^2$, $k^2 = i\omega\mu_0\sigma + \varepsilon\varepsilon_0\mu_0\omega^2$. The amplitude of the transverse $B_1$ field is a function of x only. The z component of the $B_1$ field does not contribute to spin excitation but is needed in order to satisfy the zero divergence requirement for the B field. In the following, $B_1$ refers to the transverse components of the RF field.

In the simulation, the transmit array consisted of 49 "composite excitation elements," each having three orthogonal circular current loops with axes parallel to the x, y and z directions, respectively. The diameter of each current loop was 4.7 cm. The center positions of all three loops in one composite excitation element were the same, as given in Table 1 and also demonstrated in Figure 1 for elements in the yz-plane.

The RF field calculation was performed using the finite-difference time-domain (FDTD) method [5] with self-developed software written in IDL (version 5.6, Research Systems Inc, CO). The simulations were performed on a 90x90x90 $cm^3$ volume. At the center of this volume, (x,y,z) = (0,0,0). The center of the head is located at the center of this volume as well. The size of the Yee cell was 1.5 cm. The current loops transmitted RF power from the air. The simulation calculated the RF field inside a human head template at 170 MHz with $\varepsilon = 60$ and $\sigma = 0.5$ S/m. The object was constructed based on multi-slice MR images of the head, neck and chest of an adult male. The boundary conditions of the volume of calculation were set up using the method of "perfectly matched layers" [6]. The spatial distribution of the RF field from each current loop was calculated separately. A linear least squares procedure was used to construct the desired complex vector RF field patterns in the head, defined as regions with $z > -8$ cm in the template as depicted in Figure 1, using vector addition of the fields from all the loops. There were a total of 294 variables involved in the least squares fit, including electric current amplitude and phase in each of all 49x3 loops. Finally, circularly polarized transverse $B_1$ field was obtained.

Table 1. Center positions of current loops.

| Level | z (cm)* | x and y (cm) |
|---|---|---|
| 1 | -19.9 | x = [-11.5, 0.0, 11.5, -11.5, 0.0, 11.5 ], y = [8.1, 11.5, 8.1,-13.8, -13.8, -13.8] |
| 2 | -11.5 | $x = 19.9 \cdot \sin(n\pi/6)$, $y = 19.9 \cdot \cos(n\pi/6)$, n = 0, 1, …, 11 |
| 3 | 0.0 | $x = 23.0 \cdot \sin(n\pi/6)$, $y = 23.0 \cdot \cos(n\pi/6)$, n = 0, 1, …, 11 |
| 4 | 11.5 | the same as Level 2 |
| 5 | 19.9 | $x = 11.5 \cdot \sin(n\pi/3)$, $y = 11.5 \cdot \cos(n\pi/3)$, n = 0, 1, …, 5 |
| 6 | 23.0 | x = 0.0, y = 0.0 |

* Positive z values denote the superior direction.

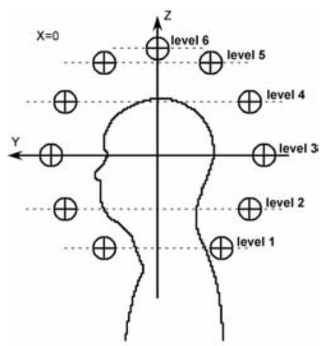


Fig. 1. Location of current loops centered in the x=0 plane.

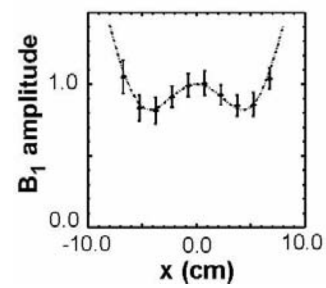


Fig. 2. Comparison of the target CP $B_1$ amplitude (dashed line) and mean ± s.d. of the field generated by the array coil in each calculated sagittal plane within a human brain.

## Results

The simulations generated $B_1$ amplitude patterns that we hoped to achieve. The dashed line in Figure 2 shows the target $B_1$ amplitude as a function of x calculated from Eq. (1) with $k_1 = 0.71 \times \sqrt{\mathrm{Re}(k^2)}$ at 170 MHz. Vertical bars in the figure show the mean ± s.d. of CP $B_1$ amplitude in each sagittal brain slice generated by the array transmit coil with $z_0 = 0$ in Eq. (1). The calculated field pattern agrees with the target field pattern with random and unbiased deviations. The standard deviation of the $B_1$ amplitude is approximately constant from plane to plane. In other simulations not described here, the calculated CP $B_1$ amplitude distribution was also close to the target field patterns.

## Discussion and Conclusions

The study demonstrated the possibility of generating analytical field patterns using an array coil configuration. Smaller in-plane coefficient of vatiation of the $B_1$ field may be achievable if the number of the composite array elements is increased. The array coil approach and the inclusion of current loops for generating and controlling the z-component of the RF field [7] offer increased flexibility in RF shimming.

In conclusion, using computer simulations we have demonstrated that parallel RF excitation with an array coil can, in principle, yield $B_1$ amplitude with a high degree of in-plane homogeneity in a 3D volume for high field MRI of the human brain.

## References

**1.** Hoult DI, J Magn Reson Imaging 2000; 12: 46-67. **2.** Foo TK, et al., Magn Reson Med 1992; 23: 287-301. **3.** Alsop DC, et al., Magn Reson Med 1998; 40: 49-54. **4.** Ibrahim TS, et al., Magn Reson Imaging 2001; 19: 1339–1347. **5.** Yee KS, IEEE Trans Antennas Propag 1966; 14: 302-307. **6.** Berenger J-P, Journal of Computational Physics 1994; 114: 185-200. **7**. Wang ZJ, et al., Magn Reson Eng 2005; 24B: 1-5.